Role of the potassium/lysine cationic center in catalysis and functional asymmetry in membrane-bound pyrophosphatases

Erika Artukka[1], Heidi H. Luoto[1], Alexander A. Baykov[2], Reijo Lahti[1] and Anssi M. Malinen[1]

[1]Department of Biochemistry, University of Turku, FIN-20014 Turku, Finland and [2]Belozersky Institute of Physico-Chemical Biology, Lomonosov Moscow State University, Moscow 119899, Russia

Correspondence: Anssi M. Malinen (email: anssi.malinen@utu.fi).

ABSTRACT
Membrane-bound pyrophosphatases (mPPases), which couple pyrophosphate hydrolysis to transmembrane transport of H^+ and/or Na^+ ions, are divided into K^+,Na^+-independent, Na^+-regulated, and K^+-dependent families. The first two families include H^+-transporting mPPases (H^+-PPases), whereas the last family comprises one Na^+-transporting, two Na^+-and H^+-transporting subfamilies (Na^+-PPases and Na^+,H^+-PPases respectively), and three H^+-transporting subfamilies. Earlier studies of the few available model mPPases suggested that K^+ binds to a site located adjacent to the pyrophosphate-binding site, but is substituted by the ε-amino group of an evolutionarily acquired lysine residue in the K^+-independent mPPases. Here, we performed a systematic analysis of the K^+/Lys cationic center across all mPPase subfamilies. An Ala→Lys replacement in K^+-dependent mPPases abolished the K^+ dependence of hydrolysis and transport activities and decreased these activities to the level (4‑7%) observed for wild-type enzymes in the absence of monovalent cations. In contrast, a Lys→Ala replacement in K^+,Na^+-independent mPPases conferred partial K^+ dependence on the enzyme by unmasking an otherwise conserved K^+-binding site. Na^+ could partially replace K^+ as activator of K^+-dependent mPPases and the Lys→Ala variants of K^+,Na^+-independent mPPases. Finally, we found that all mPPases were inhibited by excess substrate, suggesting strong negative cooperativity of active site functioning in these homodimeric enzymes; moreover, the K^+/Lys center was identified as part of the mechanism underlying this effect. These findings suggest that the mPPase homodimer possesses an asymmetry of active site performance that may be an ancient prototype of the rotational binding-change mechanism of F-type ATPases.

Abbreviations
ACMA, 9-amino-6-chloro-2-methoxyacridine; AMDP, aminomethylenediphosphonate; H^+-PPase, H^+-transporting PPase; IMVs, inverted membrane vesicles; mPPase, membrane-bound PPase; Na^+-PPase, Na^+-transporting PPase; Na^+,H^+-PPase, Na^+- and H^+-transporting PPase; PNP, imidodiphosphate; PPase, pyrophosphatase; PP_i, inorganic pyrophosphate; TMA, tetramethylammonium.

Introduction

Membrane-bound pyrophosphatases couple the hydrolysis of pyrophosphate (PP_i) to the transport of H^+ and/or Na^+ ions across membranes [1–6]. mPPases are found in most plants, algae and protists, and ~25% of bacterial and archaeal species [1], but are absent in humans and other metazoans. In many organisms, mPPases are localized to both the plasma membrane [7] and membranes of cell organelles, such as vacuoles in plants [8,9] and acidocalcisomes [10–12] in bacteria. In all cellular locations, the PP_i hydrolysis site faces the cytoplasm, and the direction of cation transport is away from the cytoplasm. mPPases advance the survival of the host organism during energy shortages and other types of stress, such as high salinity, intoxication

and drought [13–17]. The relative physiological importance of mPPase-mediated ion transport and pyrophosphatase activities may vary among host organisms and depends on growth conditions [5,18]. Nevertheless, mPPases are currently being widely employed as plant-engineering tools in agrobiotechnology [19–22]. Moreover, the presence of mPPases in several pathogenic microorganisms has prompted drug-development efforts [23].

Structurally, mPPases are relatively simple homodimeric proteins. Each ~75-kDa subunit typically contains 16 long transmembrane α-helices (**Figure 1A**) that form two concentric rings [24,25]. The inner ring consists of six helices and forms a gated ion transport funnel. The catalytic site is located at the entrance to the funnel on the cytoplasmic side of the membrane and binds PP_i and five magnesium ions, which serve as bridges between PP_i and protein groups. The nucleophilic water molecule is activated by coordination with two aspartates, as is the case in aspartyl proteases [26]. Three proposed mechanisms of mPPases [1,24,25] all assume "Mitchellian" direct coupling of hydrolysis and proton transport via the transport funnel connecting the hydrolysis site to the outer surface of the membrane, as opposed to the indirect coupling established for functionally similar H^+-ATPases [27] (see review by Walker [28] for terminology). The mechanisms, however, differ in the assumed order in which PP_i hydrolysis and transport events occur [24] and the role of the proton released during PP_i hydrolysis in Na^+ transport [1,29].

mPPases constitute a functionally diverse protein superfamily, whose members exhibit different transport specificity and requirements for alkali metal ions. Phylogenetic and functional classification of mPPase protein sequences have revealed three main protein families: K^+,Na^+-independent H^+-transporting PPases (H^+-PPases), Na^+-regulated ("divergent") H^+-PPases, and K^+-dependent mPPases (**Figure 1B**) [29]. The K^+-dependent mPPase family is further divided into five subfamilies: Na^+-transporting PPases (Na^+-PPases) [30], which can additionally transport H^+ at subphysiological Na^+ concentrations [31]; two distinct lineages of Na^+,H^+-PPases, which transport both cations under physiological conditions [32]; and three lineages of H^+-PPases [33]. The K^+-dependent H^+-PPase and Na^+,H^+-PPase subfamilies most likely evolved from Na^+-PPase ancestors through the action of independent evolutionary pathways on structural elements that determine transport specificity [33]. In addition to Mg^{2+} ions, Na^+ is also required for PP_i hydrolysis by Na^+-PPases and Na^+,H^+-PPases. K^+ is a nonessential activator of the latter mPPases, but is thought to be important for the activity of K^+-dependent H^+-PPases. Na^+-regulated H^+-PPases have no requirement for a monovalent cation; however, their activity is modulated by both Na^+ and K^+ [29].

The key determinant of K^+ dependence in mPPases, a residue in the middle of α-helix 12, is Ala in K^+-dependent mPPases and Lys in K^+-independent mPPases. Because an Ala→Lys substitution was shown to render the activity of *Carboxydothermus hydrogenoformans* H^+-PPase independent of K^+ [34], it was suggested that the ε-NH_3^+ group of Lys acts as a surrogate for the K^+ ion in K^+-independent H^+-PPases; this interpretation was later supported by modeling experiments based on the crystal structures of K^+-bound mPPases [24]. The cationic group of the K^+/Lys center forms a direct contact with the PP_i molecule [24,25] (**Figure 1C**). Side effects of K^+ in Na^+-regulated H^+-PPases include displacement of active-site–bound Mg^{2+} ions at low Mg^{2+} concentrations with concomitant modulation of the apparent PP_i hydrolysis rate [29], despite the presence of a Lys in these mPPases.

In the current study, we performed a systematic analysis of the K^+/Lys cationic center across the whole mPPase protein superfamily. We introduced K^+ signature residue reversions by creating Ala→Lys or Lys→Ala substitutions in seven mPPases, representing different mPPase families and subfamilies (**Table 1**), and determined the consequence of these substitutions for the monovalent cation and substrate dependencies of hydrolytic and transport activities. We also analyzed the role of the K^+/Lys cationic center in inter-subunit communication, inferred from inhibitory effects of excess substrate.

Experimental

Expression of mPPase genes in *Escherichia coli* and production of recombinant mPPases

mPPase genes from *Desulfitobacterium hafniense* (Dh-PPase) and *Geobacter sulfurreducens* (Gs-PPase) were amplified from genomic DNA (obtained from Leibniz Institute DSMZ - German Collection of Microorganisms and Cell Cultures) by polymerase chain reaction (PCR) and cloned into the pET36b plasmid (Novagen), in which expression is driven by the T7 promoter. Ala→Lys and Lys→Ala substitutions were generally introduced by site-directed mutagenesis using Phusion High-Fidelity DNA polymerase (ThermoFisher Scientific); the only exception was the GC-rich *G. sulfurreducens* mPPase gene, into which the Lys→Ala substitution was introduced at *Nco*I and *Sal*I restriction sites as a ~400-bp synthetic fragment (synthesized by Eurofins Genomics). Cloned wild-type and mutated mPPase gene constructs were verified by sequencing. Procedures used to prepare plasmid vectors bearing genes encoding mPPases from *Desulfuromonas acetoxidans* (Da-PPase) [33], *Bacteroides vulgatus* (Bv-PPase) [35], *Flavobacterium johnsoniae* (Fj-PPase) [33], *Leptospira biflexa* (Lb-PPase) [33], *Chlorobium limicola* (Cl(2)-PPase) [29], *Rhodospirillum rubrum* (Rr-PPase), [36] *Cellulomonas fimi* (Cf-PPase) [29] and the Na^+-PPase from *Methanosarcina mazei* (Mm-PPase) [30] were described previously.

mPPase genes were expressed in *E. coli* C41(DE3)ril cells as described previously [37]. The cells were broken using a French Press, and inverted membrane vesicles (IMVs) were isolated and washed three times by repeated ultracentrifugation/resuspension in an Na^+- and K^+-free buffer [37]. IMVs were then suspended in storage buffer (10 mM MOPS-TMA hydroxide pH 7.2, 900 mM sucrose, 5 mM DTT, 1 mM $MgCl_2$, 50 µM EGTA), and aliquots were frozen in liquid nitrogen and stored at -80 ^oC. Vesicles were quantified by determining their protein content using the Bradford assay [38]. mPPase expression was confirmed by sodium dodecyl sulfate-polyacrylamide gel electrophoresis (SDS-PAGE; GelCode Blue stain, ThermoFisher Scientific) and Western blot analysis. IMV proteins (10 µg) were separated by SDS-PAGE on 4–20% gradient gels (Precise Tris-Glycine gels, ThermoFisher Scientific) and blotted onto nitrocellulose membranes (pore size 0.45 µm). After incubation with 5% (w/vol) nonfat milk, anti-mPPase antibody [30], diluted 1/10,000, was added. After washing the membrane five times with wash buffer (0.1 M Tris-HCl pH 7.6, 0.15 M NaCl, 0.05% Tween-20), the membrane was treated with 1/5000-diluted fluorescently labeled anti-rabbit secondary antibody [IRDye 800CW Donkey Anti-Rabbit IgG (H+L) Highly Cross Adsorbed; Li-Cor], and scanned using an Odyssey infrared imager (Li-Cor). PageRuler Unstained Protein Ladder (ThermoFisher Scientific) and PageRuler Plus Prestained Protein Ladder (10 to 250 kDa; ThermoFisher Scientific) were used in Coomassie-stained and Western blotting gels, respectively.

Hydrolytic activity assay

The reaction buffer (25 ml) typically contained 0.1 M MOPS-TMA hydroxide (pH 7.2), 5 mM free Mg^{2+} ion, 40 µM EGTA and varying concentrations of TMA_4PP_i, NaCl, and KCl. The concentrations of contaminating Na^+ and K^+ ions in the assay medium were estimated to be 3 and 6 µM, respectively, using atomic absorption spectrometry. The reaction was initiated by adding IMV suspension (0.01–0.4 mg protein), and liberation of inorganic phosphate was continuously recorded for 2–3 min using a flow-through phosphate analyzer [39]. Reaction rates were calculated from the initial slopes of the P_i liberation traces. The results of duplicate measurements were usually consistent within 10%.

Cation transport measurements

mPPase-mediated H^+ transport activity was assayed using the fluorescent probe, 9-amino-6-chloro-2-methoxyacridine (ACMA), as a reporter of IMV lumen acidification [40]. The assay buffer consisted of 20 mM MOPS-TMA hydroxide (pH 7.2), 5 mM free Mg^{2+}, 300 µM Mg_2PP_i, 8 µM EGTA, 2 µM ACMA, and 0.3 mg/ml IMVs. Where indicated, 50 mM K^+ and 0.1 mM Na^+

were added. Cl^- concentration was maintained constant at 160 mM by adding TMA chloride. The reaction mixture (2 ml) was incubated for 4 min in the dark and 2 min in the light before the reaction was initiated by adding TMA_4PP_i. After 5 min, the H^+ gradient was collapsed by adding 10 mM NH_4Cl. Changes in fluorescence were recorded at excitation and emission wavelengths of 428 and 475 nm, respectively, using a PerkinElmer LS-55 spectrofluorometer.

Na^+ transport was measured using radioactive $^{22}NaCl$ (PerkinElmer) as a tracer, as previously described [30,33]. Briefly, IMVs (1 mg/ml) were incubated for 1 min at 22 ^oC in 100 mM MOPS-TMA hydroxide buffer (pH 7.2) containing 1 mM Na^+, 5 mM Mg^{2+}, 1 mM TMA_4PP_i, and 40 µM EGTA; 50 mM K^+ was included where indicated, and Cl^- ion concentration was always adjusted to 160 mM with TMA chloride. The transport reaction was initiated in a total volume of 80 µl by adding 1 mM TMA_4PP_i (or an equal volume of water in control runs). Reactions were stopped after 1 min by adding 20 mM EDTA, after which 60 µl of the suspension was vacuum filtered through a nitrocellulose filter (0.2 µm pore size, 13 mm diameter; Millipore). The filter was washed with 1 ml wash buffer (5 mM MOPS-TMA hydroxide pH 7.2, 100 mM Na^+, 0.5 mM Mg^{2+}, 160 mM TMA chloride). The amount of $^{22}Na^+$ transported inside IMVs was determined by transferring the filter to a microcentrifuge tube, adding 1 ml Ultima Gold mixture (PerkinElmer) and then performing liquid scintillation counting with a 1215 Rackbeta instrument (LKB-Wallac).

Trypsin digestion assay

mPPase sensitivity to trypsin digestion was determined in a reaction mixture (total volume, 0.1 ml) consisting of 20 mM MOPS-TMA hydroxide buffer (pH 7.2) containing 5 mM $MgCl_2$, 8 µM EGTA), 1.4 mg/ml IMVs, and 0.14 mg/ml L-1-tosylamido-2-phenylethyl chloromethyl ketone (TPCK)-treated bovine trypsin (Sigma). The low enzymatic activity of the Dh-PPase A460K variant required the use of a 1-ml assay volume. KCl (50 mM) and the non-hydrolysable substrate analogue imidodiphosphate (100 µM) were also included where indicated. Trypsin digestion was performed for 0–28 min at 37 ^oC, and aliquots ($1/10^{th}$ of the reaction volume) were withdrawn at different time points and assayed for PP_i hydrolysis activity, as indicated above. Control incubations were performed without trypsin. P_i liberation time courses were linear, indicating that dilution of proteins with the activity assay mixture effectively stopped proteolysis.

Calculations and data analysis

PP_i and Mg^{2+} form two types of complexes, $MgPP_i$ and Mg_2PP_i, the latter of which is the true substrate of mPPases [41]. In addition, free PP_i forms weaker complexes with K^+ and Na^+ [41]. The concentrations of $MgCl_2$ and TMA_4PP_i required to maintain 5 mM free Mg^{2+} ion (the essential cofactor) and necessary concentrations of the Mg_2PP_i complex at pH 7.2 were calculated as described previously, using the dissociation constants for Mg^{2+}, Na^+, K^+, and H^+ complexes of PP_i [41].

The kinetic model in **Scheme 1** was used to describe the K^+ and Na^+ dependencies of the PP_i hydrolysis reaction at saturating substrate concentration. ES represents the enzyme-substrate complex; M is K^+ or Na^+; K_1 and K_2 represent the metal binding constant; and V_0, V_1 and V_2 are the maximal velocities for the corresponding enzyme–substrate complexes. **Scheme 1** assumes that binding of the first alkali metal ion stimulates hydrolysis, whereas binding of the second metal ion inhibits it. The dependencies of PP_i hydrolysis on substrate ($S = Mg_2PP_i$) concentration were analyzed in terms of **Scheme 2**, where E_2 represents dimeric enzyme, K_{m1} and K_{m2} are microscopic Michaelis constants, and V_1 and V_2 are per-site maximal velocities for the mono- and di-substrate complexes, respectively.

$$\begin{array}{ccccc} & K_1 & & K_2 & \\ \mathrm{ES} & \leftrightarrow & \mathrm{ESM} & \leftrightarrow & \mathrm{ESM_2} \\ \downarrow V_0 & & \downarrow V_1 & & \downarrow V_2 \end{array}$$

Scheme 1. K^+ and Na^+ binding to the enzyme–substrate complex.

$$\begin{array}{ccccc} & K_{\mathrm{m1}} & & & \\ \mathrm{E_2} & \leftrightarrow & \mathrm{E_2S} & \rightarrow & V_1 \\ K_{\mathrm{m1}} \downarrow\uparrow & K_{\mathrm{m2}} & \downarrow\uparrow K_{\mathrm{m2}} & & \\ \mathrm{SE_2} & \leftrightarrow & \mathrm{SE_2S} & \rightarrow & 2V_2 \\ \downarrow V_1 & & & & \end{array}$$

Scheme 2. Substrate binding and hydrolysis at two active sites of a dimeric mPPase.

Rate equations for the mechanisms in **Schemes 1 and 2** are provided by corresponding **Equations 1 and 2**, where [M] and [S] correspond to K^+ and Na^+ and substrate concentrations, respectively. Parameter values and their standard errors were determined by fitting these equations to rate data using Scientist software (MicroMath). The equations were reduced appropriately in cases where enzyme species shown in **Schemes 1 and 2** were inactive or could be neglected for a particular mPPase.

$$v = (V_1 + V_0K_1/[\mathrm{M}] + V_2[\mathrm{M}]/K_2)/(1 + K_1/[\mathrm{M}] + [\mathrm{M}]/K_2) \quad (1)$$

$$v = (2V_1 + 2V_2[\mathrm{S}]/K_{m2})/(2 + K_{m1}/[\mathrm{S}] + [\mathrm{S}]/K_{m2}) \quad (2)$$

Results

Production of wild-type and variant mPPases

To evaluate the structural and functional conservation of the K^+ ion-binding site across the mPPase protein family, we expressed pairs of representative wild-type and variant proteins for each of the seven mPPase subfamilies (**Figure 1B**). In the variant mPPases, the K^+-signature residue was inverted from the one signifying K^+ dependence to that suggesting K^+-independent function or *vice versa*. In practice, an Ala→Lys substitution was introduced into five K^+-dependent mPPases—Da-PPase (Na^+-PPase [33]), Bv-PPase (Na^+,H^+-PPase [35]), Dh-PPase (H^+-PPase, see below), Fj-PPase (H^+-PPase [33]) and Lb-PPase (H^+-PPase [33])—and Lys→Ala substitutions were made in Gs-PPase (K^+,Na^+-independent H^+-PPase, see below) and Cl(2)-PPase (Na^+-regulated H^+-PPase [29]).

Recombinant mPPases were produced in *E. coli* and isolated as inverted membrane vesicles (IMVs). Western blot analysis using a polyclonal antibody recognizing a conserved mPPase peptide [30] revealed protein bands within the expected mPPase size range (**Figure 2A**, upper panel). Consistent with the fact that *E. coli* has no endogenous mPPase, no immunoreactive bands were detected in IMVs isolated from *E. coli* transformed with empty cloning vector. The

antibody used did not bind to the sequence-divergent Cl(2)-PPase (**Figure 2B**, upper panel, lanes 16–17), confirming a previous finding [29]. Successful expression of the wild-type and mutant Cl(2)-PPases could, however, be inferred from the appearance of ~70 kDa Coomassie-stained protein bands in SDS-PAGE gels (**Figure 2A**, lower panel, lanes 16–17) and the presence of PP_i hydrolysis activity in these IMVs, but not in native *E. coli* IMVs (**Figure 2C**). Notably, highly hydrophobic mPPases commonly migrate faster in SDS-PAGE than would be expected for soluble proteins of the same masses. As previously reported [29,30], expression levels of different mPPases varied and constituted less than 10% of total IMV protein, based on Coomassie-stained SDS-PAGE gels (**Figure 2A**, lower panel). The mutation in the K^+-signature residue did not significantly affect expression levels.

The PP_i-hydrolyzing activities of Dh-PPase and Gs-PPase, produced for the first in this study, were almost completely insensitive to fluoride, a strong inhibitor of soluble *E. coli* PPase [42], but were markedly inhibited by aminomethylenediphosphonate (AMDP), an mPPase-specific inhibitor [42] (**Figure 2B**). We conclude that all mPPases were successfully isolated as active recombinant proteins in *E. coli* IMVs.

K^+ ion as activator of wild-type and variant mPPases

The response of mPPase hydrolytic activity to K^+ ions was determined at a fixed substrate concentration (100 μM Mg_2PP_i). Because Na^+-transporting PPases always require Na^+ for catalytic activity, these PPases were assayed in the presence of 50 mM Na^+. With the exception of Gs-PPase, all wild-type enzymes were stimulated by millimolar concentrations of K^+, with saturation typically taking place at approximately 100 mM (**Figure 3**, data indicated in circles). K^+-binding affinity and degree of activation were determined from rate data in **Figure 3**, analyzed in terms of **Scheme 1** using **Equation 1** (**Table 2)**. The ratio of rates at zero and optimal K^+ concentration (V_o/V_1) was less than 1 for all Ala-containing wild-type and variant mPPases, and was lowest for the K^+-dependent H^+-PPases (Dh, Fj and Lb). Activities measured in the absence of K^+ were insensitive to 0.25 mM TMA fluoride (data not shown), ruling out contamination by *E. coli* PPase as the source of the K^+-independent activity [42]. Na^+-transporting Da-PPase and Bv-PPase exhibited higher relative activities in the absence of K^+ because the assay medium used for these enzymes contained 50 mM Na^+, which could partially fulfill the role of K^+ as activator [30,37]. Surprisingly, but in accord with our previous findings [29], K^+ moderately activated Na^+-regulated Cl(2)-PPase, despite the fact that the presence of Lys implied that this H^+-PPase is independent of K^+ ions. The K^+-insensitivity of Gs-PPase activity confirmed our phylogenetics-based prediction (**Figure 1B**) that this PPase is a member of the K^+-independent mPPase family.

The Ala→Lys substitution of K^+-dependence signature in Da-PPase, Bv-PPase, Dh-PPase, Fj-PPase, and Lb-PPase invariably eliminated the stimulatory effect of K^+ on PP_i hydrolysis activity (**Figure 3,** indicated in triangles). In the case of Fj-PPase, the Ala→Lys substitution even made K^+ a low-affinity inhibitor, possibly signifying that a K^+ ion is able to replace one of the active-site–bound Mg^{2+} ions in this mPPase, and possibly others [29]. The behavior of the Ala→Lys variants is fully consistent with the crystal structure-based prediction [24] that the ε-NH_3^+ group of the Lys structurally and functionally replaces the K^+ ion in its binding site.

Removal of the Lys residue from a K^+-independent Gs-PPase yielded a variant enzyme whose activity in the absence of K^+ was only ~5% that of the wild-type enzyme, but was increased at moderate [K^+], indicating appearance of a K^+-binding site in the variant Gs-PPase. The Lys thus contributes to, but is not essential for, the activity of K^+-independent H^+-PPases. However, activity was restored to its original value at high K^+ concentrations (compare V_0/V_1 and V_2/V_1 in **Table 2**). The observation that the Lys→Ala substitution in Cl(2)-PPase rendered the activity more responsive to K^+ compared with the wild-type enzyme (5-fold vs. 2-fold stimulation) and increased the K^+-binding affinity (K_a) 4-fold supports the presence of a Lys-masked K^+-binding site also in Na^+-regulated H^+-PPases.

Lys substitutes for K^+ as a facilitator of Na^+ binding in variant Na^+-PPases

K^+ has a dual role in the activation of Na^+-transporting mPPases, increasing both the maximal rate of PP_i hydrolysis and Na^+-binding affinity in almost all cases tested [30,33,37]. Data shown in **Figure 4** reproduce the trend for the wild-type Da-PPase (Na^+-PPase) by showing a 2.5-fold higher maximal activity (V_1 in **Table 3**) and 10-fold smaller Na^+-binding constant (K_1 in **Table 3**) in the presence of 50 mM K^+. K^+ also strongly stimulated Na^+ binding (60-fold) in Bv-PPase (Na^+,H^+-PPase), but without significantly affecting the maximal catalytic rate.

The Ala→Lys substitution abolished both aforementioned K^+ roles in Da-PPase and Bv-PPase. The Na^+ activation curves for variant Da-PPase and Bv-PPase were nearly identical in the presence and absence of 50 mM K^+, suggesting that these PPases lack the K^+-binding site. Accordingly, the Na^+-binding constants (K_1) in **Table 3** closely matched the values determined for the wild-type enzymes in the presence of K^+. This observation indicates that introduction of Lys into the K^+ signature position precisely mimics K^+ binding in the wild-type enzymes, producing a concomitant increase in Na^+-binding affinity in Na^+-PPases and Na^+,H^+-PPases.

The activity of wild-type Gs-PPase was not affected by Na^+, whereas the activity of Cl(2)-PPase was inhibited by Na^+ (**Figure 4**), consistent with their identification as K^+,Na^+-independent and Na^+-regulated mPPases, respectively. The Lys→Ala substitution, however, conferred partial Na^+ activation to both PPases in the absence of K^+, possibly indicating that Na^+ replaces K^+ in this capacity in the unmasked K^+-binding site. High Na^+ concentrations were inhibitory in the variant Gs-PPase and restored its original activity, as was described above for the K^+ effect. The effects of Na^+ were reproducible with different IMV batches.

The Lys ε-NH_3^+ group mimics K^+ as activator of the ion transport function

Here, we evaluated the impact of K^+ and K^+ signature residue substitution on the ion transport activities of mPPases. H^+ pumping was measured in the presence and absence of 50 mM K^+ using ACMA as a fluorescent reporter of IMV lumen pH [40] (**Figure 5**). Addition of PP_i to the assay mixture initiated H^+-transport into the IMV lumen for all mPPases, as indicated by the quenching of ACMA fluorescence. The H^+-transport activity of the Na^+-transporting Da-PPase is consistent with the earlier finding that Na^+-PPases can transport protons at sub-physiological Na^+ concentrations [31]. The fluorescence intensity returned to its initial level following the addition (at ~7 min) of the proton gradient disruptor, ammonium chloride. The initial rate and maximal level of fluorescence quenching were strongly dependent on the presence of 50 mM K^+ in the case of wild-type K^+-dependent mPPases (Da, Bv, Dh, Fj and Lb). In contrast, the H^+-transport activities of Gs-PPase (K^+,Na^+-independent H^+-PPase) and Cl(2)-PPase (Na^+-regulated H^+-PPase) were K^+-independent. The Ala→Lys substitution rendered H^+-transport much less dependent on K^+, whereas the Lys→Ala substitution increased its dependence on K^+.These effects paralleled those of the corresponding substitutions on the PP_i hydrolysis activity of mPPases (**Figures 3 and 4**). Furthermore, all the Ala→Lys-substituted mPPases demonstrated increased H^+-transport activities by comparison with the wild-type forms assayed in the absence of K^+. This finding indicated that the introduced Lys partially substituted for K^+ as the activator of the transport function.

The Na^+-transport activity of wild-type and Ala→Lys-substituted Na^+-PPase (Da-PPase) and Na^+,H^+-PPase (Bv-PPase) was determined using $^{22}Na^+$ as a tracer (**Figure 6**). All four enzyme forms mediated Na^+ accumulation into the lumen of IMVs in the presence of PP_i. Addition of 50 mM K^+ to the assay medium increased the amount of Na^+ transported inside IMVs by 4–9-fold in wild-type enzymes, but had no effect in the Ala→Lys variants. These results are again consistent with the effects of K^+ on PP_i hydrolysis by these enzymes (**Figures 3 and 4**). The Na^+-transport activity of the variant Da-PPase was greater than that of the wild-type enzyme assayed in the absence of K^+, signifying the ability of the Lys to partially substitute for K^+ as the activator, also in Na^+-transport. A similar but smaller effect was observed with Bv-PPase (**Figure 6**). Noteworthy, Na^+-transport rates were greater with Da-PPase than with the

corresponding forms of Bv-PPase, consistent with higher activity of the former enzyme in PP_i hydrolysis (**Figures 3 and 4**).

All H^+-PPases characterized to date fail to transport detectable amounts of Na^+ into IMVs, implying that these enzymes possess a strict Na^+-exclusion mechanism [29,33]. The Ala→Lys-substituted Lb-PPase was also incapable of Na^+ transport (**Figure 6**). These findings indicate that the occupancy or structure of the K^+-binding site does not directly contribute to the mechanism, efficiency, or specificity of H^+- and Na^+-transport reactions.

Kinetic cooperativity in mPPases and its dependence on the K^+/Lys cationic center

Interestingly, all wild-type enzymes were inhibited at high (>100 μM) substrate concentrations in the presence of 50 mM K^+ (**Figure 7**). The inhibition was the smallest with Dh-PPase (15 %) but reproducible, also with different IMV batches. A similar substrate inhibition was observed in the Na^+-PPase from *M. mazei*, the K^+,Na^+-independent H^+-PPase from *R. rubrum*, and the Na^+-regulated H^+-PPase from *C. fimi* (profiles not shown). This effect was analyzed in terms of **Scheme 2**, which assumes different kinetic behaviors of the two otherwise identical active sites in the mPPase homodimer. Specifically, substrate binding to one site changes the K_m value and maximal velocity for the second site. With wild-type Dh-PPase, fitting to the simple Michaelis-Menten equation resulted in a 10 times greater sum of the squares of residuals, confirming that this mPPase is also susceptible to substrate inhibition. The qualitative effects seen in **Figure 7** and the parameter values estimated using **Equation 2** (**Table 4**) indicate that the substrate molecule bound to one site impedes binding of the second substrate molecule by a factor of 1.5‑38 and slows substrate conversion at both sites in the E_2S_2 complex by 3‑16-fold.

In K^+-free medium, substrate inhibition was not observed with any wild-type K^+-dependent mPPase, including H^+-transporting (Dh, Fj and Lb) and Na^+-transporting (Da and Bv) enzymes (**Figure 7**). In these experiments, the Na^+-dependent Bv-PPase and Da-PPase were assayed in the presence of 10 mM Na^+ to maintain their activity; as described above, Na^+ was expected to occupy K^+-binding sites in the absence of K^+. Nonetheless, a similar lack of substrate inhibition of Bv-PPase was observed at 1 and 100 mM Na^+, the concentrations at which K^+-binding sites are expected to be predominantly empty or Na^+-bound, respectively. A likely corollary is that mere occupancy of the cationic center is insufficient for the substrate inhibition to take place – the ligand should be K^+ and not Na^+.

The Lys-containing K^+-independent mPPases (Gs, Rr, Cl(2) and Cf) were most sensitive to substrate inhibition, an observation that is highly compatible with the presence of a charged amino group in the cationic center. However, the Ala→Lys substitution abolished substrate inhibition in all tested K^+-dependent mPPases, except Dh-PPase, suggesting that inter-subunit communication imposes more subtle structural requirements on the configuration of the amino acid residue network around the K^+/Lys center.

Consistent with the proposed role of the K^+/Lys center in substrate inhibition, and hence inter-subunit communication, the K^+,Na^+-independent Gs-PPase and Na^+-regulated Cl(2)-PPase, which have Lys and do not bind K^+, exhibited substrate inhibition both in the presence and absence of K^+. This again means that the ε-NH_3^+ group of Lys in authentic Lys-containing mPPases can functionally substitute for K^+ both in catalysis and inter-subunit communication. Consistent with this interpretation, the Lys→Ala variants of these mPPases exhibited no substrate inhibition.

K^+ binding does not affect the overall structure of Dh-PPase

Given the role of the K^+-binding site in catalysis and inter-subunit communication in mPPases, we explored the effect of K^+ binding on gross protein conformation in Dh-PPase, using the sensitivity of PPase activity to trypsin digestion as an indicator. The wild-type and variant enzymes lost their activities at similar rates during incubation with trypsin, and the rates were not significantly affected by 50 mM K^+ (**Figure 8**). In contrast, addition of the substrate analogue

imidodiphosphate fully protected both enzyme forms against trypsin-mediated inactivation, both in the presence and absence of K^+. We conclude that K^+ binding to or residue substitution at the binding site does not significantly affect protein conformation, at least not in a manner that changes the accessibility of Lys and Arg residues to trypsin.

Discussion

The division of membrane-bound PPases into independently evolving K^+-dependent and K^+-independent families has long been recognized. The major effects of K^+ are to increase the maximal activity in all K^+-dependent mPPases and to increase Na^+-binding affinity in Na^+-transporting mPPases [30–34]. No 3D structure of a K^+-independent mPPase has yet been experimentally solved, but structural modeling suggests that the ε-NH_3^+ group of the introduced Lys reaches towards the normal K^+ ion binding site, thereby mimicking its activating functions [24]. However, the mechanistic basis of the K^+-dependence and its change during the evolution of mPPase families and subfamilies has remained incompletely understood. In this study, we addressed these questions by performing mutagenesis of the key K^+-dependence determinant—the Ala/Lys cationic center—in mPPases of all subfamilies and characterizing the functional properties of the wild-type and variant proteins.

Three different effects of the Ala→Lys substitution were observed. First, the K^+ ion lost its potency as an activator in all Ala→Lys-substituted mPPases, consistent with the original report that this substitution abolishes K^+ dependence in *C. hydrogenoformans* H^+-PPase [34]. Second, Ala→Lys variants exhibited greatly decreased catalytic activities — 4–7% of the wild-type activity. Interestingly, also the PP_i hydrolysis and proton transport activities of wild-type K^+-dependent H^+-PPases had similar magnitudes in the absence of K^+ ions. Two likely corollaries are that K^+ is a modulator, rather than an absolute requirement, and that several Ala→Lys-substituted mPPases hydrolyze PP_i predominantly via the low-activity "K^+-unbound" pathway. Further evidence in favor of the co-existing "K^+-bound" and "K^+-unbound" pathways in PP_i hydrolysis and ion transport is provided by Lys→Ala-substituted Gs-PPase (wild-type is K^+,Na^+-independent) and Cl(2)-PPase (wild-type is Na^+-regulated): both enzymes exhibited significant activity in the absence of K^+, but were further activated (2.2–5.2-fold) in its presence. Furthermore, the Ala→Lys variant of *C. hydrogenoformans* H^+-PPase, which belongs to the same subfamily as Dh-PPase (**Figure 1B**), exhibited 50% of the activity of the wild-type enzyme [34]. The degree of catalytic compensation provided by the introduced Lys thus seems to vary from enzyme to enzyme instead of correlating with the specific mPPase subfamily. In the crystal structure of a plant H^+-PPase, the K^+ ion was shown to interact with bound imidodiphosphate/PP_i [25], thereby increasing its electrophilicity and providing an additional contact with the enzyme. The former effect seems to depend more on the precise positioning of the K^+/Lys cationic center, because the substitutions and/or K^+ removal had only a small effect on the PP_i-binding affinity (as characterized by K_m value), but largely, and to a variable degree, suppressed the catalytic activity.

Finally, Ala→Lys substitutions in Na^+-PPases and Na^+,H^+-PPases faithfully mimicked the K^+-induced increase in Na^+-binding affinity. Thus, the mechanism by which the K^+/Lys cationic center stimulates Na^+ binding appears to be more tolerant to variations in the binding pose of the ε-NH_3^+ group of Lys compared with K^+. The exact mechanism remains undefined, but takes place across a significant distance, as bound K^+ and Na^+ ions are separated by ~16 Å [43].

The K^+-independent H^+-PPases are regarded as descendants of K^+-dependent mPPases [33,36], which have a functional K^+ binding site. If so, stimulation of the Lys→Ala variants by K^+ indicates that the overall configuration of the K^+-binding site remained unchanged during the divergent evolution to K^+-independent H^+-PPases, but the site became occupied by a Lys side chain. The Lys→Ala substitution thus only restored a preexisting functional K^+-binding site in these enzymes. Such strong selection against an evolutionary change can be rationalized in terms of the ε-NH_3^+ group of Lys indeed being a structural and functional equivalent of the K^+ ion in

K^+-independent H^+-PPases [24,34]. Interestingly, bound K^+ ion locates in a water-filled cavity in the 3D structure of *Vigna radiata* H^+-PPase [25] and interacts weakly with an asparagine residue and PP_i (interatom distances of 3.4 Å). Such an arrangement may indeed allow this site to accommodate different cations (K^+, Na^+, NH_4^+) that optimize mPPase function. Importantly and consistent with our interpretation, the amino acid residues forming the cavity (Asp530, Gly533 and Asn534, *V. radiata* mPPase numbering) are absolutely conserved between all mPPase families.

An unusual feature of the K^+-binding site created in Gs-PPase is that enzyme activation by K^+ is only observed at moderate, but not high, K^+ concentrations. This may mean that the activation results from K^+ binding to one subunit and vanishes when both subunits are occupied by K^+ in the dimeric enzyme.

Subunit interdependence in mPPases is also suggested by the dependence of activity on substrate concentration. All wild-type mPPases are prone to inhibition by excess substrate, which decreases the PP_i hydrolysis rate to 6−35 % of its maximum value. Importantly, the H^+ transport activity of Cl(2)-PPase is also strongly inhibited by excess substrate [29], again demonstrating the tight connection between PP_i hydrolysis and ion transport. A similar inhibitory effect of excess substrate was previously reported by Leigh et al. for an oat vacuolar K^+-dependent mPPase [44]. Inspection of the 3D structure of mPPases [24,25,43] reveals that the hydrolytic center and ion conductance funnel lack the space to accommodate a second PP_i molecule and that no potential binding cavity is present elsewhere in the protein. Clearly, the inhibition results from substrate binding to the second active site in the enzyme dimer. This is consistent with the dependence of substrate inhibition on the state of the K^+/Lys center, because this dependence implies a tight mechanistic connection, and hence physical proximity, of the sites that accommodate both PP_i molecules and the K^+/Lys center. With the K^+-dependent mPPases, excess substrate inhibition was only observed in the K^+-bound state; enzymes with vacant or Na^+-occupied K^+-binding site, as well as Ala→Lys-substituted enzymes, were not susceptible to excess substrate inhibition. The variant Dh-PPase was the only exception, indicating that the position of the amino group introduced with Lys perfectly matches that of K^+ in authentic Dh-PPase. Consistent with this interpretation, authentic Gs-PPase and Cl(2)-PPase, containing Lys in the K^+/Lys center, were inhibited by excess substrate both in the absence and presence of K^+. However, K^+ could not replace Lys in this capacity in the Lys→Ala variants of these PPases, again indicating the absence of a perfect match between the two cationic groups in the authentic enzymes and their variants.

We hypothesize that substrate binding to one active site distorts the conformation of the other site, thereby hampering its interaction with substrate, as evidenced by an increased K_m value. Furthermore, subsequent substrate binding to the second active site removes structural asymmetry by partially reversing the strain on the first active site, thereby diminishing the catalytic constants for both sites ($V_2 < V_1$ in **Table 4**). Consistent with this interpretation, X-ray crystallography studies indicate no significant structural asymmetry in mPPases in which both active sites are vacant [24] or substrate-bound [25,43]; however, no structure of an mPPase in which half the sites are occupied is available to fully test our hypothesis. The dual effects of K^+ and Na^+ on the Lys→Ala variant of Gs-PPase, which acquired a single cation-binding site per subunit upon amino acid replacement, can also be rationalized in terms of this mechanism. Subunit interdependence in mPPases is also indicated by the observation that inactivation of one subunit in the enzyme dimer by radiation-induced destruction or site-directed mutagenesis is sufficient to compromise the enzymatic activity of the intact partner subunit [45–47]. The induced asymmetry can also explain the observed half-of-the-sites reactivity of plant mPPase in modification by fluorescein isothiocyanate [48].

How could negative kinetic cooperativity contribute to the mPPase mechanism? First, cooperativity implies that only one active site in the enzyme dimer predominantly operates at any given time at moderate PP_i concentrations. No asymmetry is seen in the substrate-free state, suggesting that the sites may undergo a “flip-flop” in the next catalytic cycle. This substrate-

induced asymmetry is reminiscent of the Boyer's "binding-change" mechanism of F-type ATPase, in which three active sites cyclically adopt three different conformations with different affinities for the substrate [49]. The F-ATPase molecule has a cyclic symmetry, and the sequential binding change is achieved through proton-driven rotation of the γ-subunit within the ball-shaped structure formed by three pairs of catalytic α- and β-subunits [49,28,50]. This allows conversion of the energy released upon H^+ or Na^+ transport into conformational energy, which, in turn, is used for ATP synthesis from ADP and P_i (and *vice versa* in the reverse process). Notably, mPPases are also reversible transporters and can utilize an [H^+] gradient to synthesize PP_i [51]. Although a similar rotation is impossible in an mPPase, its two subunits may instead undergo the above-described oscillations between two conformations. This mechanism would use conformational energy less efficiently, but might still suffice for the transport reactions driven by PP_i hydrolysis, which releases two times less energy than ATP hydrolysis [52]. Accordingly, the transport stoichiometry exceeds 3 cations per ATP molecule for F-ATPase [28], but is only 1–2 for mPPases [53–55].

The structural basis for the interdependence of mPPase subunits is not entirely clear and will require further study. Most of the dimer interphase is formed by transmembrane helices 10 and 13 [25]. Based on the functional consequences of amino acid substitutions in this area (enzyme inactivation or partial decoupling of hydrolysis from transport [56]) and the observed conformational change upon PP_i binding [43], it was suggested that helices 10 and/or 13 mediate the motions of the inner helix ring to the outer ring and further into the neighboring subunit [43]. How bound K^+ can control these rearrangements is even less clear. Single-molecule FRET measurements of the distances between corresponding residues in two subunits of *Clostridium tetani* mPPase (later identified as an Na^+-PPase [57,58]) and studies testing protection of Dh-PPase against trypsin digestion revealed no conformational change upon K^+ binding.

In summary, our study demonstrates the evolutionary and mechanistic conservation of the K^+-binding site and the signature Ala/Lys residue across the mPPase protein superfamily. The evolutionary steps that resulted in divergence of K^+-dependent and K^+-independent families apparently magnified the catalytic potency of the preexisting K^+-free catalytic pathway through acquisition of a K^+-mimicking Lys residue near the K^+-binding site [34]. Furthermore, kinetic analyses revealed a K^+/Lys center-mediated negative cooperativity of active site function in homodimeric mPPases, possibly indicating that mPPases utilize an ancient prototype of the rotational binding-change mechanism of F-type ATPase.

Acknowledgments

We are grateful to Edita Jetullahi Mulaku and Laura Kovesjoki for their skillful technical assistance with the cloning and expression of mPPases. We also thank Dr Alexander Bogachev for the Na^+ and K^+ analyses.

Competing interests

The authors declare that there are no competing interests associated with the manuscript.

Funding

This work was supported by grants from the Academy of Finland (307775), the Russian Foundation for Basic Research (15-04-04828), and the Ministry of Education and the Academy of Finland (to the National Graduate School in Informational and Structural Biology). A.M.M. was additionally supported by the Instrufoundation (Instrumentariumin tiedesäätiö) and the Finnish cultural foundation (Suomen Kulttuurirahasto). H.H.L was additionally supported by the Emil Aaltonen foundation (Emil Aaltosen säätiö) and Turku University foundation (Turun Yliopistosäätiö).

Author Contribution

E.A. and H.H.L. performed the experiments. All authors were involved in designing the study, interpreting the results, and writing the manuscript.

References

1 Baykov, A. A., Malinen, A. M., Luoto, H. H. and Lahti, R. (2013) Pyrophosphate-fueled Na^+ and H^+ transport in prokaryotes. *Microbiol. Mol. Biol. Rev.* **77**, 267–276

2 Tsai, J. Y., Kellosalo, J., Sun, Y. J. and Goldman, A. (2014) Proton/sodium pumping pyrophosphatases: The last of the primary ion pumps. *Curr. Opin. Struct. Biol.* **27**, 38–47

3 Serrano, A., Pérez-Castiñeira, J., Baltscheffsky, M. and Baltscheffsky, H. (2007) H^+-PPases: yesterday, today and tomorrow. *IUBMB Life* **59**, 76–83

4 Drozdowicz, Y. M. and Rea, P. A. (2001) Vacuolar H(+) pyrophosphatases: from the evolutionary backwaters into the mainstream. *Trends Plant Sci.* **6**, 206–211

5 Maeshima, M. (2000) Vacuolar H(+)-pyrophosphatase. *Biochim. Biophys. Acta* **1465**, 37–51

6 Gaxiola, R. A., Palmgren, M. G. and Schumacher, K. (2007) Plant proton pumps. *FEBS Lett.* **581**, 2204–2214

7 Martinez, R., Wang, Y., Benaim, G., Benchimol, M., de Souza, W., Scott, D. A. and Docampo, R. (2002) A proton pumping pyrophosphatase in the Golgi apparatus and plasma membrane vesicles of *Trypanosoma cruzi*. *Mol. Biochem. Parasitol.* **120**, 205–213

8 Rea, P. A. and Poole, R. J. (1993) Vacuolar H^+-translocating pyrophosphatase. *Annu. Rev. Plant Physiol. Plant Mol. Biol* **44**, 157–180

9 Li, J., Yang, H., Peer, W. A., Richter, G., Blakeslee, J., Bandyopadhyay, A., Titapiwantakun, B., Undurraga, S., Khodakovskaya, M., Richards, E. L., Krizek, B., Murphy, A. S., Gilroy, S. and Gaxiola, R. (2005) *Arabidopsis* H^+-PPase AVP1 regulates auxin-mediated organ development. *Science* **310**, 121–125

10 Scott, D. A., de Souza, W., Benchimol, M., Zhong, L., Lu, H. G., Moreno, S. N. and Docampo, R. (1998) Presence of a plant-like proton-pumping pyrophosphatase in acidocalcisomes of *Trypanosoma cruzi*. *J. Biol. Chem.* **273**, 22151–22158

11 Docampo, R. and Moreno, S. N. J. (2011) Acidocalcisomes. *Cell Calcium* **50**, 113–119

12 Docampo, R., de Souza, W., Miranda, K., Rohloff, P. and Moreno, S. N. (2005) Acidocalcisomes - conserved from bacteria to man. *Nat. Rev. Microbiol.* **3**, 251–261

13 Gaxiola, R. A., Li, J., Undurraga, S., Dang, L. M., Allen, G. J., Alper, S. L. and Fink, G. R. (2001) Drought- and salt-tolerant plants result from overexpression of the AVP1 H^+-pump. *Proc. Natl. Acad. Sci. U. S. A* **98**, 11444–11449

14 Gamboa, M. C., Baltierra, F., Leon, G. and Krauskopf, E. (2013) Drought and salt tolerance enhancement of transgenic *Arabidopsis* by overexpression of the vacuolar pyrophosphatase 1 (EVP1) gene from Eucalyptus globulus. *Plant Physiol. Biochem.* **73**, 99–105

15 Yang, Y., Liu, Y., Yuan, H., Liu, X., Gao, Y., Gong, M. and Zou, Z. (2016) Membrane-bound pyrophosphatase of human gut microbe *Clostridium methylpentosum* confers improved salt tolerance in *Escherichia coli*, *Saccharomyces cerevisiae* and tobacco. *Mol. Membr. Biol.* **33**, 39–50

16 Bao, A. K., Wang, S. M., Wu, G. Q., Xi, J. J., Zhang, J. L. and Wang, C. M. (2009) Overexpression of the *Arabidopsis* H^+-PPase enhanced resistance to salt and drought stress in transgenic alfalfa (*Medicago sativa L.*). *Plant Sci.* **176**, 232–240

17 Hernández, A., Herrera-Palau, R., Madroñal, J. M., Albi, T., López-Lluch, G., Perez-Castiñeira, J. R., Navas, P., Valverde, F. and Serrano, A. (2016) Vacuolar H^+-pyrophosphatase AVP1 is involved in amine fungicide tolerance in *Arabidopsis thaliana*

and provides tridemorph resistance in yeast. *Front. Plant Sci.* **7**:85

18 Ferjani, A., Segami, S., Horiguchi, G., Muto, Y., Maeshima, M. and Tsukaya, H. (2011) Keep an eye on PP_i: the vacuolar-type H^+-pyrophosphatase regulates postgerminative development in *Arabidopsis*. *Plant Cell* **23**, 2895–2908

19 Brini, F., Hanin, M., Mezghani, I., Berkowitz, G. A. and Masmoudi, K. (2007) Overexpression of wheat Na^+/H^+ antiporter TNHX1 and H^+-pyrophosphatase TVP1 improve salt- and drought-stress tolerance in *Arabidopsis thaliana* plants. *J. Exp. Bot.* **58**, 301–308

20 Pasapula V, Shen G, Kuppu S, Paez-Valencia J, Mendoza M, Hou P, Chen J, Qiu X, Zhu L, Zhang X, Auld D, Blumwald E, Zhang H, Gaxiola R, Payton P (2011) Expression of an *Arabidopsis* vacuolar H^+-pyrophosphatase gene (AVP1) in cotton improves drought- and salt tolerance and increases fibre yield in the field conditions. *Plant Biotechnol J.* **9**, 88–99

21 Gaxiola, R. A., Sanchez, C. A., Paez-Valencia, J., Ayre, B. G. and Elser, J. J. (2012) Genetic manipulation of a "vacuolar" H^+-PPase: from salt tolerance to yield enhancement under phosphorus-deficient soils. *Plant Physiol.* **159**, 3–11

22 Schilling, R. K., Marschner, P., Shavrukov, Y., Berger, B., Tester, M., Roy, S. J. and Plett, D. C. (2014) Expression of the *Arabidopsis vacuolar* H^+-pyrophosphatase gene (AVP1) improves the shoot biomass of transgenic barley and increases grain yield in a saline field. *Plant Biotechnol. J.* **12**, 378–386

23 Shah, N., Vidilaseris, K., Xhaard, H. and Goldman, A. (2016) Integral membrane pyrophosphatases: a novel drug target for human pathogens? *AIMS Biophys.* **3**, 171–194

24 Kellosalo, J., Kajander, T., Kogan, K., Pokharel, K. and Goldman, A. (2012) The structure and catalytic cycle of a sodium-pumping pyrophosphatase. *Science* **337**, 473–476

25 Lin, S. M., Tsai, J. Y., Hsiao, C. D., Huang, Y. T., Chiu, C. L., Liu, M. H., Tung, J. Y., Liu, T. H., Pan, R. L. and Sun, Y. J. (2012) Crystal structure of a membrane-embedded H^+-translocating pyrophosphatase. *Nature* **484**, 399–403

26 Meek, T. D. (1998) Catalytic mechanisms of the aspartic proteases. In Comprehensive biological catalysis (Sinnott, M., ed.), pp 327–344

27 Boyer, P. D. (1997) The ATP synthase—a splendid molecular machine. *Annu. Rev. Biochem.* **66**, 717–749

28 Walker, J. E. (2013) The ATP synthase: the understood, the uncertain and the unknown. *Biochem. Soc. Trans.* **41**, 1–16

29 Luoto, H. H., Nordbo, E., Malinen, A. M., Baykov, A. A. and Lahti, R. (2015) Evolutionarily divergent, Na^+-regulated H^+-transporting membrane-bound pyrophosphatases. *Biochem. J.* **467**, 281–291

30 Malinen, A. M., Belogurov, G. A., Baykov, A. A. and Lahti, R. (2007) Na^+-pyrophosphatase: a novel primary sodium pump. *Biochemistry* **46**, 8872–8878

31 Luoto, H. H., Nordbo, E., Baykov, A. A., Lahti, R. and Malinen, A. M. (2013) Membrane Na^+-pyrophosphatases can transport protons at low sodium concentrations. *J. Biol. Chem.* **288**, 35489–35499

32 Nordbo, E., Luoto, H. H., Baykov, A. A., Lahti, R. and Malinen, A. M. (2016) Two independent evolutionary routes to Na^+/H^+ cotransport function in membrane pyrophosphatases. *Biochem. J.* **473**, 3099–3111

33 Luoto, H. H., Belogurov, G. A., Baykov, A. A., Lahti, R. and Malinen, A. M. (2011) Na^+-translocating membrane pyrophosphatases are widespread in the microbial world and evolutionarily precede H^+-translocating pyrophosphatases. *J. Biol. Chem.* **286**, 21633–21642

34 Belogurov, G. A. and Lahti, R. (2002) A lysine substitute for K^+. A460K mutation eliminates K^+ dependence in H^+-pyrophosphatase of *Carboxydothermus hydrogenoformans*. *J. Biol. Chem.* **277**, 49651–49654

35 Luoto, H. H., Baykov, A. a, Lahti, R. and Malinen, A. M. (2013) Membrane-integral pyrophosphatase subfamily capable of translocating both Na^+ and H^+. *Proc. Natl. Acad.*

Sci. U. S. A. **110**, 1255–1260
36 Belogurov, G. A., Turkina, M. V., Penttinen, A., Huopalahti, S., Baykov, A. A. and Lahti, R. (2002) H^+-pyrophosphatase of *Rhodospirillum rubrum*. High yield expression in *Escherichia coli* and identification of the Cys residues responsible for inactivation by mersalyl. *J. Biol. Chem.* **277**, 22209–22214
37 Belogurov, G. A., Malinen, A. M., Turkina, M. V, Jalonen, U., Rytkonen, K., Baykov, A. A. and Lahti, R. (2005) Membrane-bound pyrophosphatase of *Thermotoga maritima* requires sodium for activity. *Biochemistry* **44**, 2088–2096.
38 Bradford, M. M. (1976) A rapid and sensitive method for the quantitation of microgram quantities of protein utilizing the principle of protein-dye binding, *Anal. Biochem.* **72**, 248–254
39 Baykov, A. A. and Avaeva, S. M. (1981) A simple and sensitive apparatus for continuous monitoring of orthophosphate in the presence of acid-labile compounds. *Anal. Biochem* **116**, 1–4
40 Casadio, R. (1991) Measurements of transmembrane pH differences of low extents in bacterial chromatophores. *Eur. Biophys. J.* **19**, 189–201
41 Baykov, A. A., Bakuleva, N. P. and Rea, P. A. (1993) Steady-state kinetics of substrate hydrolysis by vacuolar H^+-pyrophosphatase. *Eur. J. Biochem.* **217**, 755–762
42 Baykov, A. A., Dubnova, E. B., Bakuleva, N. P., Evtushenko, O. A., Zhen, R. G. and Rea, P. A. (1993) Differential sensitivity of membrane-associated pyrophosphatases to inhibition by diphosphonates and fluoride delineates two classes of enzyme. *FEBS Lett.* **327**, 199–202
43 Li, K.-M., Wilkinson, C., Kellosalo, J., Tsai, J.-Y., Kajander, T., Jeuken, L. J. C., Sun, Y.-J. and Goldman, A. (2016) Membrane pyrophosphatases from *Thermotoga maritima* and *Vigna radiata* suggest a conserved coupling mechanism. *Nat. Commun.* **7:**13596
44 Leigh, R. A., Pope, A. J., Jennings, I. R., Sanders (1992) Kinetics of the vacuolar H^+-pyrophosphatase: the roles of magnesium, pyrophosphate, and their complexes as substrates, activators, and inhibitors. *Plant Physiol.* **100**, 1698–1705
45 Tzeng, C. M., Yang, C. Y., Yang, S. J., Jiang, S. S., Kuo, S. Y., Hung, S. H., Ma, J. T. and Pan, R. L. (1996) Subunit structure of vacuolar proton-pyrophosphatase as determined by radiation inactivation. *Biochem. J.* **316**, 143–147
46 Wu, J. J., Ma, J. T. and Pan, R. L. (1991) Functional size analysis of pyrophosphatase from *Rhodospirillum rubrum* determined by radiation inactivation. *FEBS Lett.* **283**, 57–60
47 Sarafian, V., Potier, M. and Poole, R. J. (1992) Radiation-inactivation analysis of vacuolar H^+-ATPase and H^+-pyrophosphatase from *Beta vulgaris L*. Functional sizes for substrate hydrolysis and for H^+ transport. *Biochem. J.* **283**, 493–497
48 Yang, S. J., Jiang, S. S., Van, R. C., Hsiao, Y. Y. and Pan, R. L. (2000) A lysine residue involved in the inhibition of vacuolar H^+-pyrophosphatase by fluorescein 5'-isothiocyanate. *Biochim. Biophys. Acta - Bioenerg.* **1460**, 375–383
49 Boyer, P. D. (1993) The binding change mechanism for ATP synthase–some probabilities and possibilities. *Biochim. Biophys. Acta - Bioenerg.* **1140**, 215–250
50 Noji, H., Yasuda, R., Yoshida, M. and Kinosita, K. (1997) Direct observation of the rotation of F1-ATPase. *Nature* **386**, 299–302
51 Baltscheffsky, H., Von Stedingk, L. V, Heldt, H. W. and Klingenberg, M. (1966) Inorganic pyrophosphate: formation in bacterial photophosphorylation. *Science* **153**, 1120–1122
52 Heinonen, J. K. (2001) Biological role of inorganic pyrophosphate. *Kluwer Academic Publishers*
53 Schmidt, A. L. and Briskin, D. P. (1993) Energy transduction in tonoplast vesicles from red beet. *Arch. Biochem. Biophys.* **301**, 165–173
54 Nakanishi, Y., Yabe, I. and Maeshima, M. (2003) Patch clamp analysis of a H^+ pump heterologously expressed in giant yeast vacuoles. *J. Biochem.* **134**, 615–623

55 Sosa, A. and Celis, H. (1995) H^+/PP_i stoichiometry of membrane-bound pyrophosphatase of *Rhodospirillum rubrum*. *Arch. Biochem. Biophys.* **316**, 421–427

56 Hirono, M., Nakanishi, Y. and Maeshima, M. (2007) Identification of amino acid residues participating in the energy coupling and proton transport of *Streptomyces coelicolor A3(2)* H^+-pyrophosphatase. *Biochim. Biophys. Acta - Bioenerg.* **1767**, 1401–1411

57 Huang, Y. T., Liu, T. H., Chen, Y. W., Lee, C. H., Chen, H. H., Huang, T. W., Hsu, S. H., Lin, S. M., Pan, Y. J., Hsu, I. C., et al. (2010) Distance variations between active sites of H(+)-pyrophosphatase determined by fluorescence resonance energy transfer. *J. Biol. Chem.* **285**, 23655–23664

58 Huang, Y.-T., Liu, T.-H., Lin, S.-M., Chen, Y.-W., Pan, Y.-J., Lee, C.-H., Sun, Y.-J., Tseng, F.-G. and Pan, R.-L. (2013) Squeezing at entrance of proton transport pathway in proton-translocating pyrophosphatase upon substrate binding. *J. Biol. Chem.* **288**, 19312–19320.

Table 1 Major mPPases used in this study

mPPase abbreviation	Organism and strain	NCBI GenBank number	Subfamily / transported cation	K^+ requirement	Signature residue
Da-PPase	*D. acetoxidans* DSM684	ZP01313190	Na^+-PPase / Na^+	yes	Ala451
Bv-PPase	*B. vulgatus* ATCC8482	YP001299560	Na^+,H^+-PPase / Na^+ and H^+	yes	Ala485
Dh-PPase*	*D. hafniense* Y51	BAE86625	*C. hydrogenoformans* type / H^+	yes	Ala465
Fj-PPase	*F. johnsoniae* UW101	YP001193830	*F. johnsoniae* type / H^+	yes	Ala495
Lb-PPase	*L. biflexa* Patoc 1 (Paris)	YP001840784	plant type / H^+	yes	Ala480
Gs-PPase*	*G. sulfurreducens* PCA	NP954331	K^+,Na^+-independent / H^+	no	Lys460
Cl(2)-PPase	*C. limicola* DSM245	ACD90242	Na^+-regulated / H^+	no	Lys553

* This mPPase was produced for the first time in this work.

Table 2 Kinetic parameters for K^+ activation of PP_i hydrolysis at fixed Mg_2PP_i concentration (100 μM)

Enzyme	V_0, nmol min^{-1} mg^{-1}	V_1, nmol min^{-1} mg^{-1}	V_2, nmol min^{-1} mg^{-1}	K_1, mM
Da[†]	160 ± 10	1360 ± 20		43 ± 2
Da (A451K)[*]	67 ± 2			
Bv[†]	130 ± 10	320 ± 10		7 ± 2
Bv (A485K)[*]	21 ± 1			
Dh	40 ± 10	970 ± 40		8 ± 1
Dh (A460K)	61 ± 1			
Fj	20 ± 6	1170 ± 20		17 ± 1
Fj (A495K)	70 ± 3	<20		>100
Lb	25 ± 6	570 ± 20		6 ± 1
Lb (A480K)	23 ± 1			
Gs	700 ± 20			
Gs (K460A)	31 ± 2	70 ± 6	36 ± 3	16 ± 5[†]
Cl(2)	230 ± 10	420 ± 50		90 ± 50
Cl(2) (K553A)	21 ± 2	109 ± 4		23 ± 4

[*] The assay mixture additionally contained 50 mM Na^+.

[†] K_1 and K_2 values were arbitrarily assumed to be equal.

Table 3 Kinetic parameters for Na^+ activation/inhibition of PP_i hydrolysis at fixed Mg_2PP_i concentration (100 μM)[*]

Enzyme	V_0, nmol min^{-1} mg^{-1}		V_1, nmol min^{-1} mg^{-1}		V_2, nmol min^{-1} mg^{-1}		K_1, mM		K_2, mM	
	$-K^+$	$+K^+$	$-K^+$	$+K^+$	$-K^+$	$+K^+$	$-K^+$	$+K^+$	$-K^+$	$+K^+$
Da	<20	40 ± 20	430 ± 20	1090 ± 30			50 ± 10	5.2 ± 0.6		
Da (A451K)	<5	<5	88 ± 3	91 ± 3			4.8 ± 0.6	5.0 ± 0.6		
Bv	<10	26 ± 5	280 ± 30	270 ± 20			28 ± 6	0.44 ± 0.09		
Bv (A485K)	5 ± 1	6 ± 2	22 ± 3	22 ± 2			0.8 ± 0.3	0.7 ± 0.2	160 ± 50	170 ± 60
Dh	30 ± 10	970 ± 100	390 ± 30				25 ± 6			
Dh (A460K)	70 ± 10	80 ± 10					>500	>500		
Fj	<10	960 ± 20	180 ± 50		<10		40 ± 20	180 ± 30	120 ± 60	
Fj (A495K)	74 ± 3	70 ± 1	<10	<10			110 ± 20	100 ± 10		
Lb	20 ± 5	460 ± 50	290 ± 10		<30		60 ± 20		100 ± 50	
Lb (A480K)	22 ± 1	21 ± 1	< 5	<5			190 ± 30	140 ± 20		
Gs	630 ± 10	670 ± 10								
Gs (K460A)	27 ± 1	40 ± 2	60 ± 3		28 ± 12		29 ± 5[†]		29 ± 5[†]	
Cl(2)[‡]	220 ± 10	220 ± 10	<10	<10			80 ± 10	60 ± 10		
Cl(2) (K553A)[‡]	20 ± 2	90 ± 10	65 ± 7	<3			60 ± 30		51 ± 5	

[*]Columns designated as "$-K^+$" and "$+K^+$" show values measured in the absence and presence of 50 mM K^+, respectively.

[†]K_1 and K_2 values were arbitrarily assumed to be equal.

[‡] Parameters were calculated assuming dependence of inhibition on $[Na]^2$, as described previously for this mPPase [29].

Table 4 Kinetic parameters describing dependence of PP_i hydrolysis rate on substrate concentration*

Enzyme	$[Na^+]$, mM	V_1, nmol min^{-1} mg^{-1}		V_2, nmol min^{-1} mg^{-1}		K_{m1}, μM		K_{m2}, μM	
		$-K^+$	$+K^+$	$-K^+$	$+K^+$	$-K^+$	$+K^+$	$-K^+$	$+K^+$
Da	10	49 ± 1	780 ± 20		180 ± 60	4.6 ± 0.7	9 ± 1		340 ± 200
Da A451K	10	62 ± 1	67 ± 2			3.5 ± 0.2	5.1 ± 0.6		
Bv	1	4.5 ± 1				28 ± 10			
Bv	10	60 ± 2	280 ± 10		60 ± 40	13 ± 4	23 ± 2		800 ± 500
Bv	100	95 ± 4				14 ± 2			
Bv A485K	10	22 ± 1	18 ± 1			12 ± 3	18 ± 7		
Dh		12 ± 1	1020 ± 50		350 ± 20	19 ± 7	14 ± 2		90 ± 40
Dh A460K		78 ± 2	70 ± 3	25 ± 2	20 ± 3	2.1 ± 0.2	3.3 ± 0.4	110 ± 50	160 ± 90
Fj		6 ± 1	1150 ± 40		320 ± 30	45 ± 20	15 ± 2		150 ± 60
Fj A495K		58 ± 1	59 ± 1			2.7 ± 0.3	4.3 ± 0.5		
Lb		7 ± 1	620 ± 20		150 ± 10	16 ± 7	9.0 ± 0.6		110 ± 20
Lb A480K		18 ± 1	16 ± 1			1.5 ± 0.2	2.5 ± 0.5		
Gs		1140 ± 40	1100 ± 40	150 ± 20	100 ± 20	12 ± 1	13 ± 1	80 ± 20	110 ± 20
Gs K460A		30 ± 1	46 ± 1			27 ± 3	42 ± 3		
Cl2		600 ± 30	590 ± 50	26 ± 3	36 ± 6	39 ± 3	33 ± 5	35 ± 4	50 ± 10
Cl2 K553A		20 ± 1	100 ± 20			24 ± 4	32 ± 2		
Mm	10		270 ± 10		30 ± 10		9.2 ± 0.6		300 ± 100
Rr			340 ± 10		34 ± 4		4.2 ± 0.4		70 ± 10
Cf			90 ± 40		8 ± 3		16 ± 2		120 ± 35

*Columns designated as "$-K^+$" and "$+K^+$" show values measured in the absence and presence of 50 mM K^+, respectively. Where indicated, the assay mixture additionally contained Na^+.

FIGURE LEGENDS

Figure 1. mPPase structure and phylogeny.
(A) The 3D structure of the vacuolar *Vigna radiata* mPPase dimer (PDB ID: 4A01) [25] complexed with imidodiphosphate (red/blue sticks), K^+ ion (violet sphere), and five Mg^{2+} ions (green spheres). Two identical subunits are shown in different colors. (B) The phylogenetic tree of mPPase protein sequences, adapted from Luoto et al. [29]. Different subfamilies are depicted by color coding, and the proteins characterized in this study are identified by name; mPPases of *Thermotoga maritima* (Tm-PPase) and *V. radiata* (Vr-PPase) with known 3D structures are also shown. The physiological transport specificity of K^+-dependent mPPases is indicated in parentheses. Scale bar represents 0.4 substitutions per amino acid residue. Panels (A) and (B) were created using PYMOL (PyMOL Molecular Graphics System, version 1.5.0.4; Schrödinger, LLC, Portland, OR, USA, https://pymol.org/2/support.html#page-top). (C) Part of the structure showing coordination of the K^+ ion with distances (Å). Ala537 is the residue replaced by Lys in K^+-independent mPPases. The K^+ ligand Asn534 is absolutely conserved in all mPPase types.

Figure 2. Production of representative mPPases from each subfamily.
(A) Western blot analysis using an anti-mPPase antibody (upper panel) and Coomassie staining (lower panel; putative mPPase bands indicated by boxes) of *E. coli* membrane proteins separated by SDS-PAGE. Sizes of reference molecular mass markers are in kDa. Sequence-predicted mPPase masses are as follows: Da-PPase, 66 kDa; Bv-PPase, 77 kDa; Dh-PPase, 69 kDa; Fj-PPase, 89 kDa; Lb-PPase, 74 kDa; Gs-PPase, 70 kDa; Cl(2)-PPase, 87 kDa. (B, C) PP_i hydrolysis activities of wild-type mPPases and all mutants, measured in 100 mM MOPS-TMA hydroxide buffer (pH 7.2), 50 mM KCl, 5.3 mM $MgCl_2$, 158 µM TMA_4PP_i, and 40 µM EGTA. In the case of Da-PPase and Bv-PPase, 10 mM NaCl was additionally included. The inhibitors, potassium fluoride (250 µM) and AMDP (20 µM), were also present where indicated.

Figure 3. K^+ dependence of PP_i hydrolysis by wild-type and variant enzymes.
The reaction buffer contained 100 mM MOPS-TMA hydroxide (pH 7.2), 5.3 mM $MgCl_2$, 158 µM TMA_4PP_i, 40 µM EGTA and 0–200 mM KCl; 50 mM NaCl was also added for Da-PPase and Bv-PPase. The curves show the best fit to **Equation 1**. "Wt" stands for wild type.

Figure 4. Na^+ dependence of PP_i hydrolysis by wild-type and variant enzymes.
The reaction buffer contained 100 mM MOPS-TMA hydroxide (pH 7.2), 5.3 mM $MgCl_2$, 158 µM TMA_4PP_i, 40 µM EGTA and either 0 or 50 mM KCl. The curves show the best fit to **Equation 2**.

Figure 5. H^+ pumping by wild-type and variant mPPases.
H^+-transport reactions were initiated by the addition of PP_i. The addition of ammonium chloride at ~7 min collapsed the generated H^+ gradient. K^+ concentration was either 0 ("-K") or 50 mM ("+K"); the assay media for Da-PPase and Bv-PPase additionally contained 1 mM Na^+. Results were reproducible between different IMV batches; typical results are shown.

Figure 6. Na^+ pumping by wild-type and variant mPPases.
The reaction was performed in the absence (-) or presence (+) of 50 mM K^+. Bars show the standard deviation of three separate measurements.

Figure 7. Substrate dependence of PP_i hydrolysis by wild-type and variant enzymes.
The reaction buffer contained 100 mM MOPS-TMA hydroxide (pH 7.2), 5–7.6 mM $MgCl_2$, 0.8–1580 µM TMA_4PP_i, 40 µM EGTA and either 0 or 50 mM KCl; the assay buffer additionally

contained 10 mM NaCl for Da-PPase and Bv-PPases. The curves show the best fits to **Equation 2**.

Figure 8. Effect of K^+ and substrate analogue on the time course of mPPase digestion by trypsin, as determined by monitoring enzymatic activity. The upper and lower panels show the data measured in the absence and presence of 0.1 mM imidodiphosphate, respectively. The activity measured before trypsin addition was taken as 100 %.

Figure 1

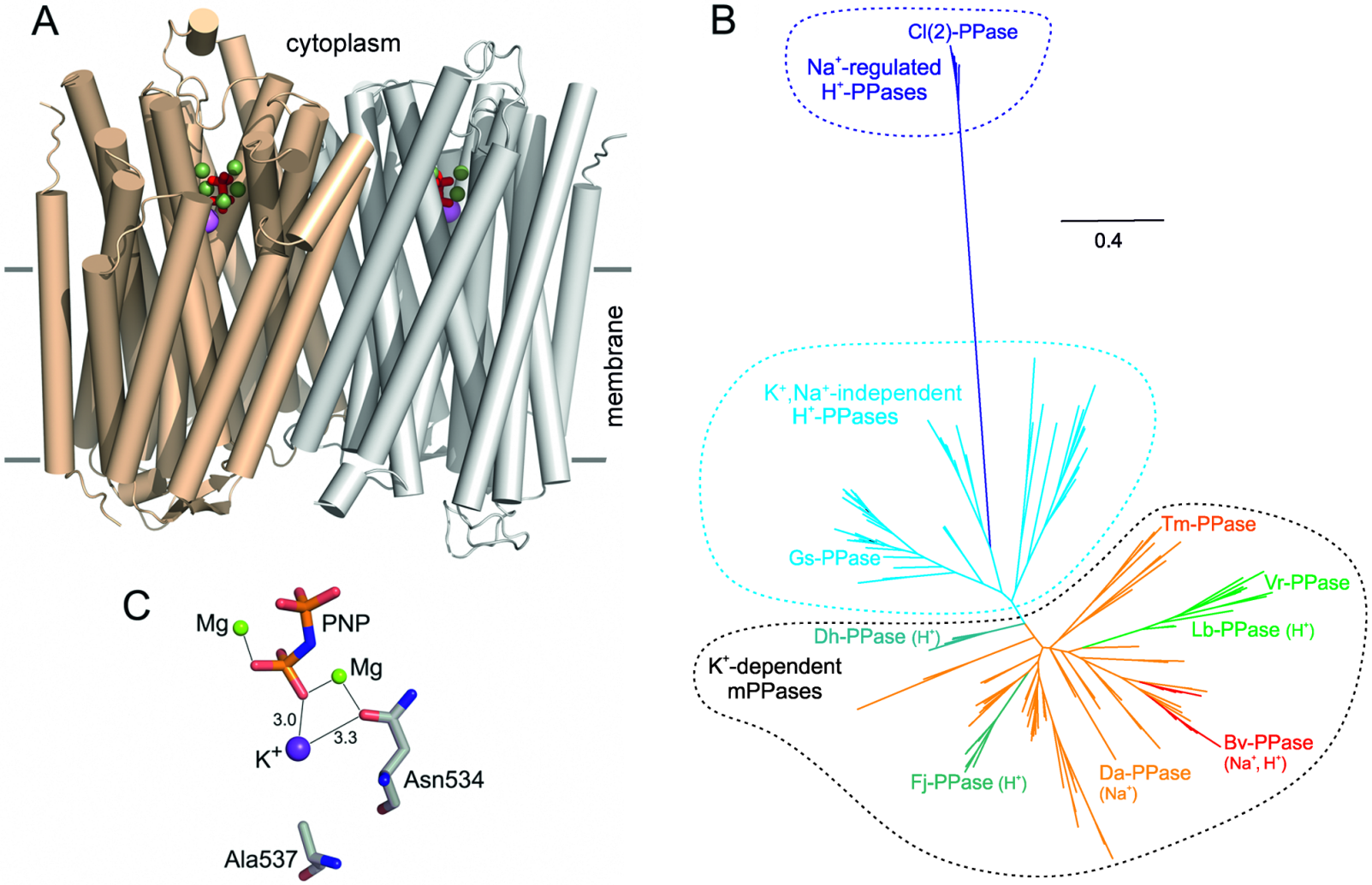
A
cytoplasm
membrane
B
Cl(2)-PPase
Na+-regulated
H+-PPases
0.4
K+,Na+-independent
H+-PPases
Gs-PPase
Tm-PPase
Vr-PPase
Lb-PPase (H+)
Dh-PPase (H+)
K+-dependent
mPPases
Bv-PPase
(Na+, H+)
Da-PPase
(Na+)
Fj-PPase (H+)
C
Mg
PNP
Mg
3.0
3.3
K+
Asn534
Ala537

Figure 2

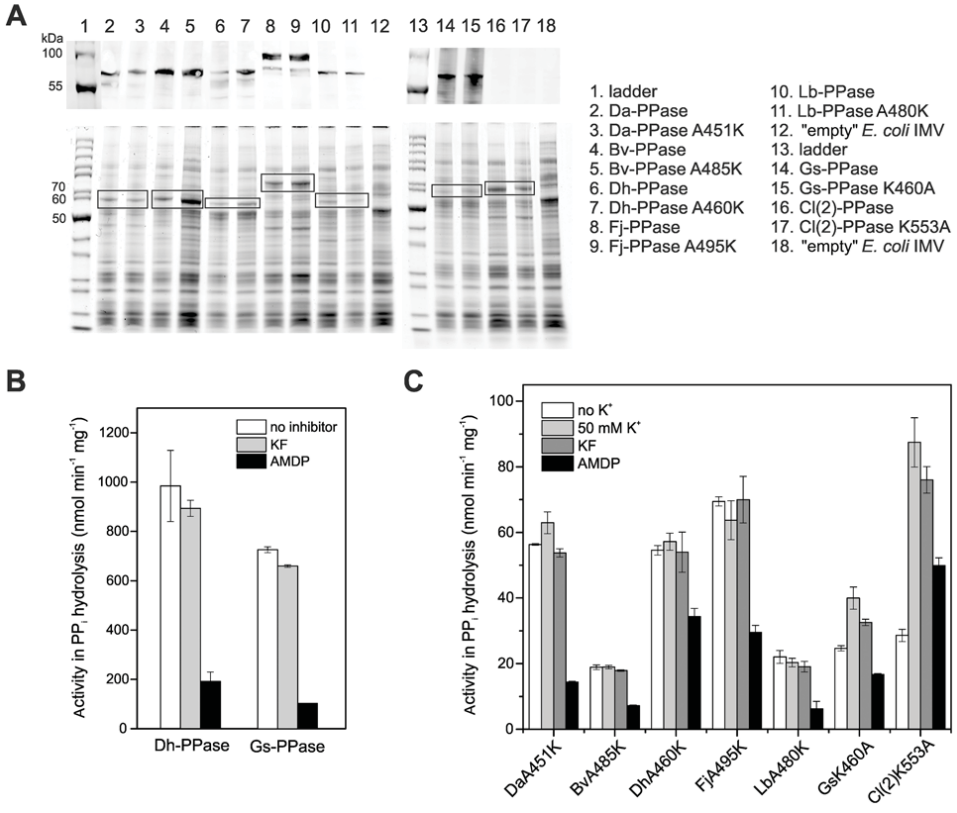
A
1 2 3 4 5 6 7 8 9 10 11 12 13 14 15 16 17 18
kDa
100
55
70
60
50
1. ladder
2. Da-PPase
3. Da-PPase A451K
4. Bv-PPase
5. Bv-PPase A485K
6. Dh-PPase
7. Dh-PPase A460K
8. Fj-PPase
9. Fj-PPase A495K
10. Lb-PPase
11. Lb-PPase A480K
12. "empty" E. coli IMV
13. ladder
14. Gs-PPase
15. Gs-PPase K460A
16. Cl(2)-PPase
17. Cl(2)-PPase K553A
18. "empty" E. coli IMV
B
Activity in PPi hydrolysis (nmol min-1 mg-1)
no inhibitor
KF
AMDP
Dh-PPase
Gs-PPase
C
Activity in PPi hydrolysis (nmol min-1 mg-1)
no K+
50 mM K+
KF
AMDP
DaA451K
BvA485K
DhA460K
FjA495K
LbA480K
GsK460A
Cl(2)K553A

Figure 3.

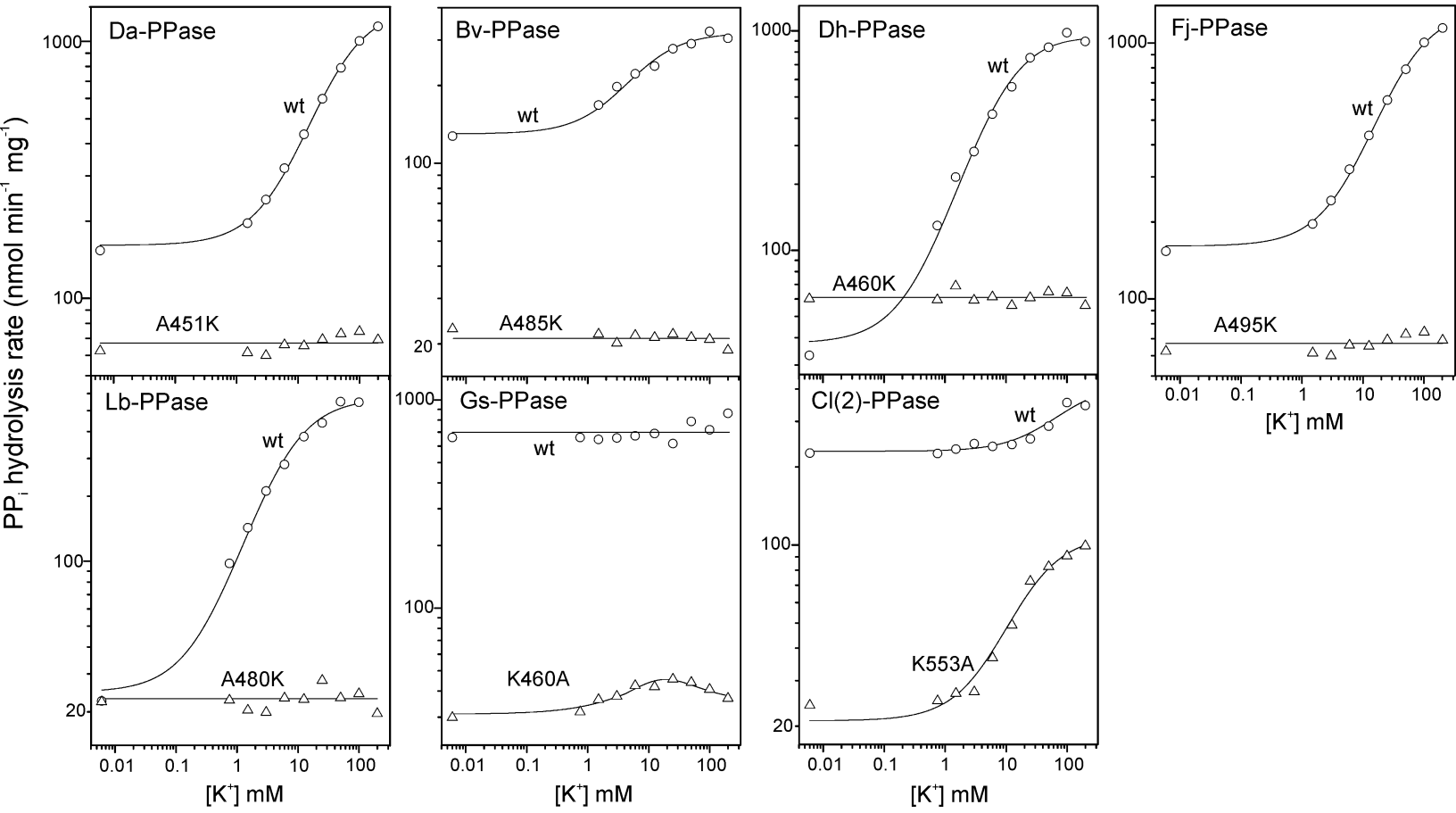
Da-PPase
wt
A451K
Bv-PPase
wt
A485K
Dh-PPase
wt
A460K
Fj-PPase
wt
A495K
Lb-PPase
wt
A480K
Gs-PPase
wt
K460A
Cl(2)-PPase
wt
K553A
1000
100
20
0.01
0.1
1
10
100
[K+] mM
PPi hydrolysis rate (nmol min-1 mg-1)

Figure 4.

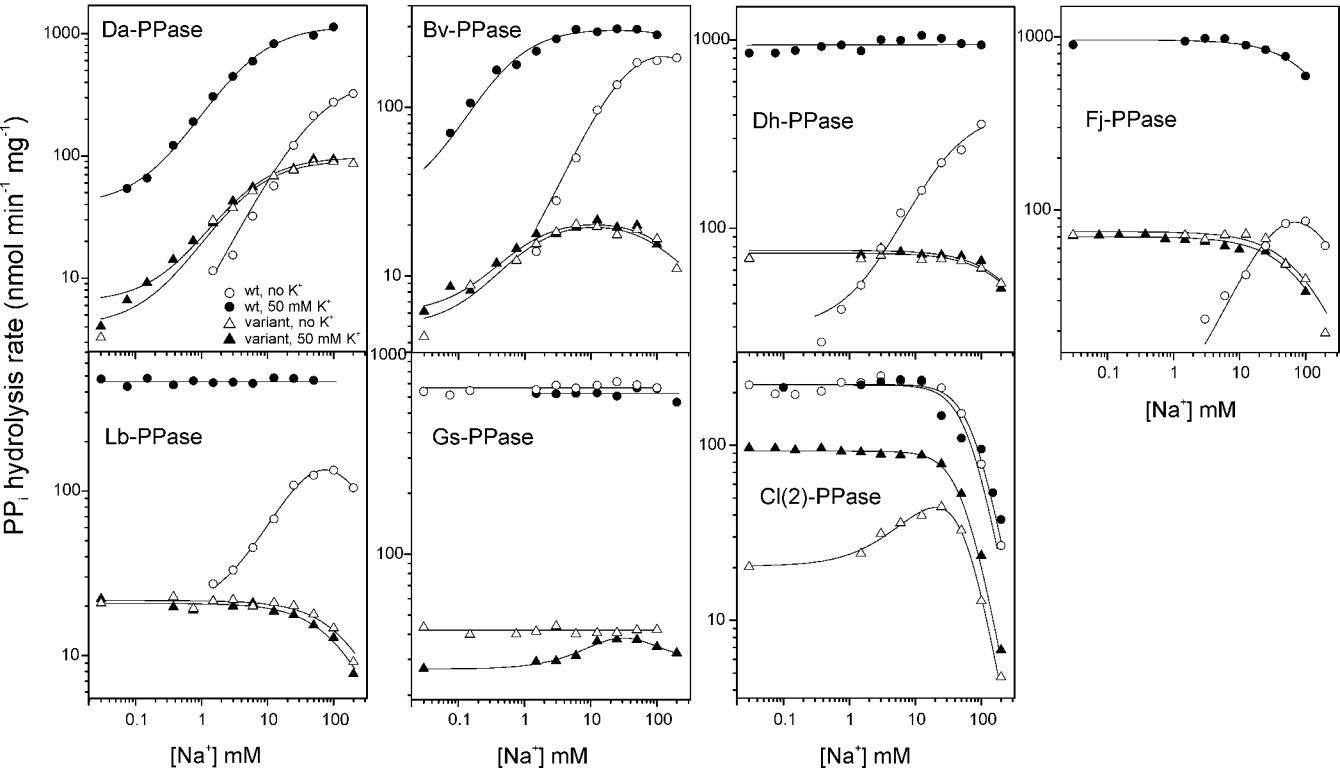
Da-PPase
Bv-PPase
Dh-PPase
Fj-PPase
Lb-PPase
Gs-PPase
Cl(2)-PPase
wt, no K+
wt, 50 mM K+
variant, no K+
variant, 50 mM K+
PPi hydrolysis rate (nmol min-1 mg-1)
[Na+] mM
1000
100
10
0.1
1
10
100

Figure 5

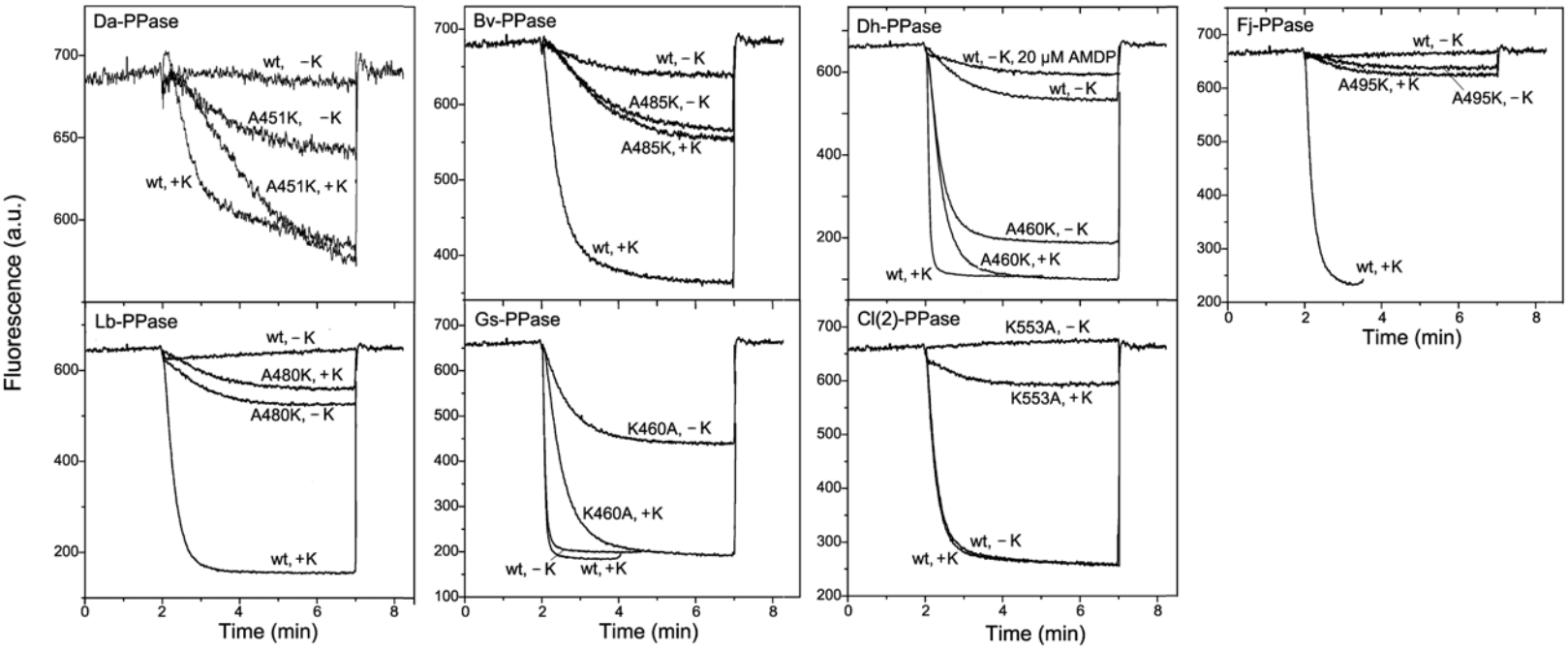
Da-PPase
wt, −K
A451K, −K
wt, +K
A451K, +K
Lb-PPase
wt, − K
A480K, + K
A480K, − K
wt, +K
Bv-PPase
wt, − K
A485K, − K
A485K, + K
wt, +K
Gs-PPase
K460A, − K
K460A, +K
wt, − K
wt, +K
Dh-PPase
wt, − K, 20 μM AMDP
wt, − K
A460K, − K
A460K, + K
wt, +K
Cl(2)-PPase
K553A, − K
K553A, + K
wt, − K
wt, +K
Fj-PPase
wt, − K
A495K, + K
A495K, − K
wt, +K
Fluorescence (a.u.)
Time (min)

Figure 6

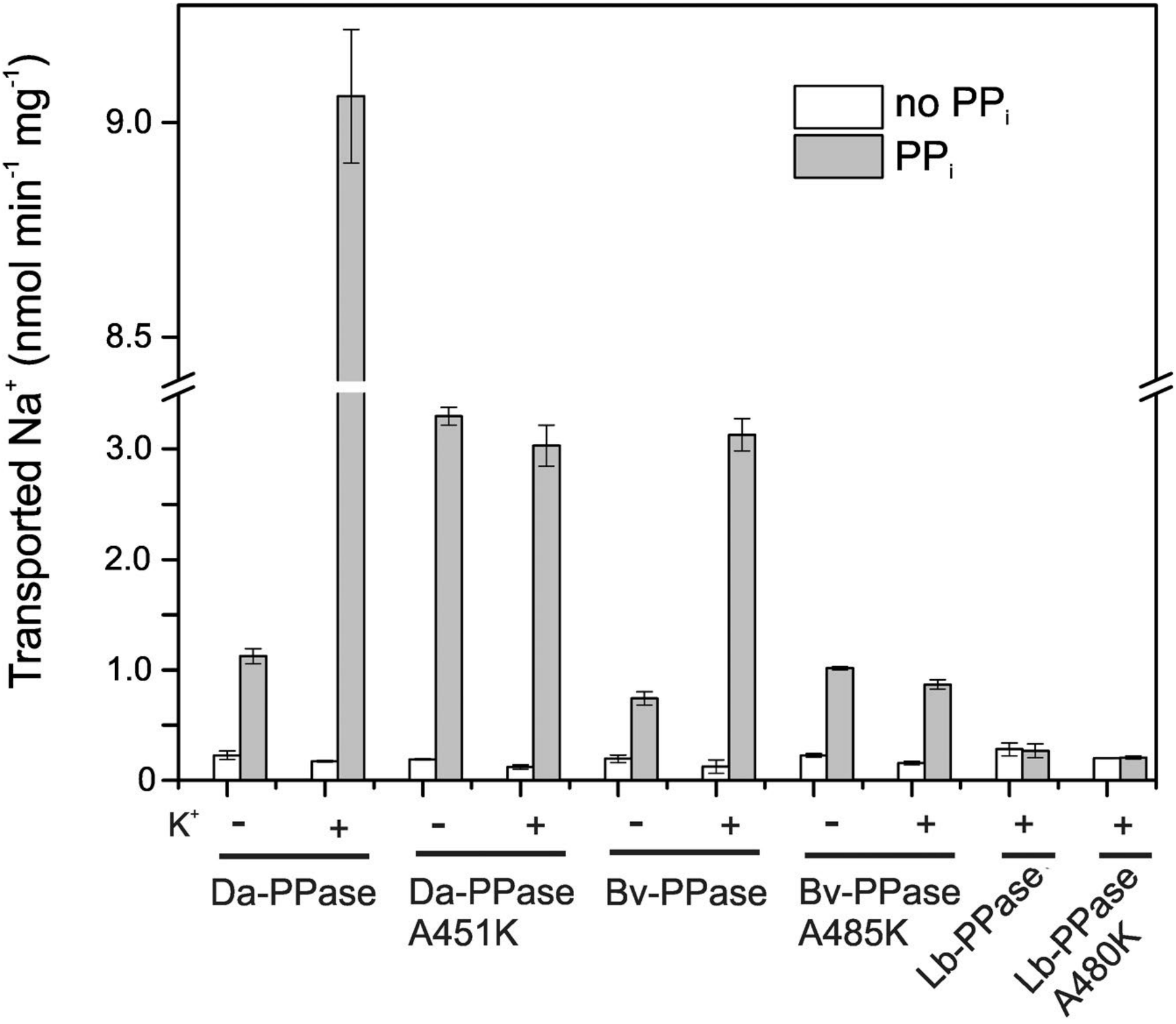
Transported Na+ (nmol min-1 mg-1)
9.0
8.5
3.0
2.0
1.0
0
no PPi
PPi
K+
-
+
-
+
-
+
-
+
+
+
Da-PPase
Da-PPase A451K
Bv-PPase
Bv-PPase A485K
Lb-PPase
Lb-PPase A480K

Figure 7

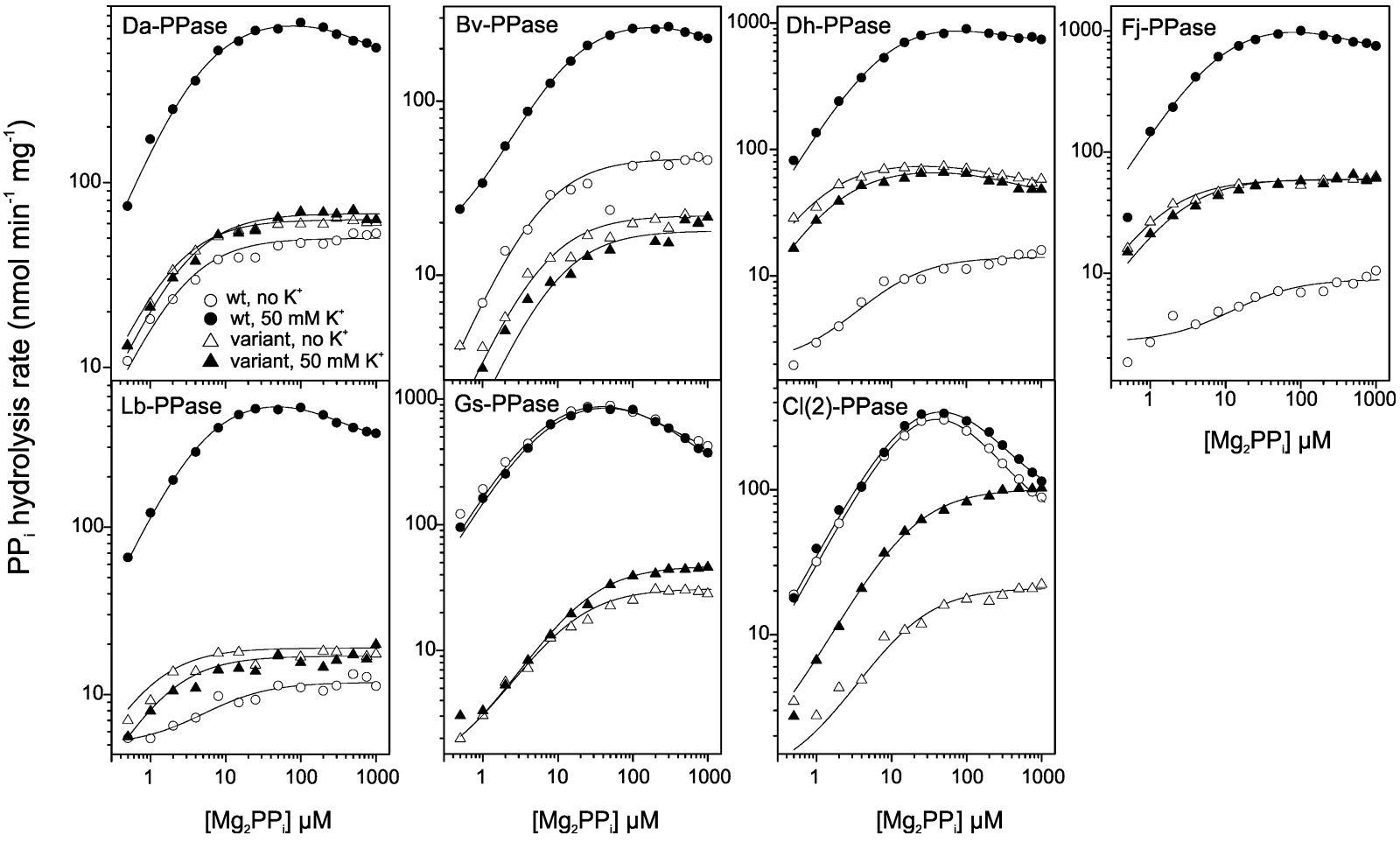
Da-PPase
Bv-PPase
Dh-PPase
Fj-PPase
Lb-PPase
Gs-PPase
Cl(2)-PPase
wt, no K+
wt, 50 mM K+
variant, no K+
variant, 50 mM K+
PPi hydrolysis rate (nmol min-1 mg-1)
[Mg2PPi] μM
10
100
1000
1
10
100
1000

Figure 8

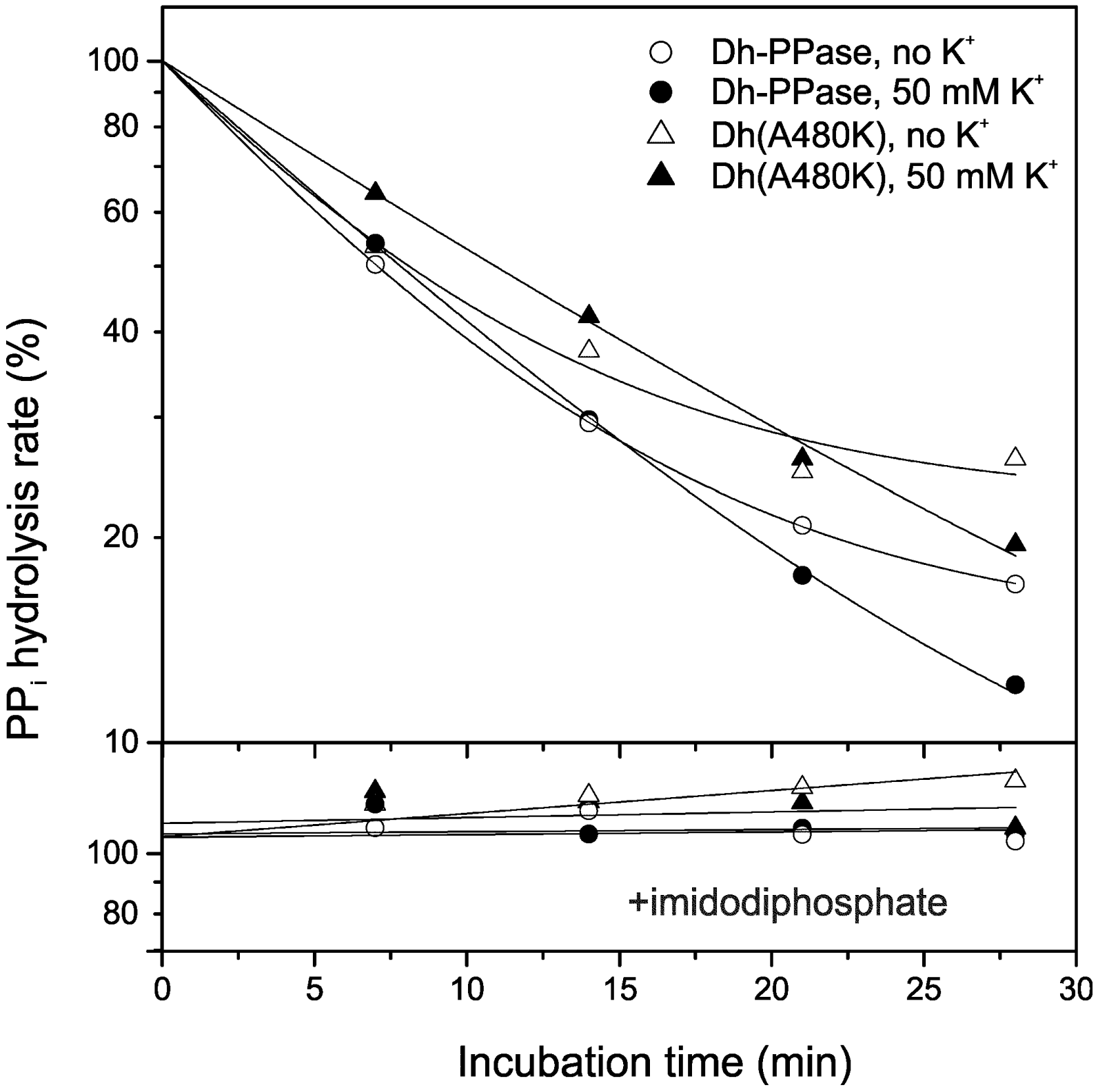
Dh-PPase, no K+
Dh-PPase, 50 mM K+
Dh(A480K), no K+
Dh(A480K), 50 mM K+
PPi hydrolysis rate (%)
100
80
60
40
20
10
100
80
+imidodiphosphate
0
5
10
15
20
25
30
Incubation time (min)